Modeling of CW Yb-doped fiber lasers with highly nonlinear cavity dynamics

S. K. Turitsyn,[1,*] A. E. Bednyakova,[2,3] M. P. Fedoruk,[2,3] A. I. Latkin,[2,3] A. A. Fotiadi,[4] A. S. Kurkov,[5] and E. Sholokhov[5]

[1]*Photonics Research Group, School of Engineering and Applied Science, Aston University, Birmingham B4 7ET, UK*
[2]*Institute of Computational Technologies, Novosibirsk, 630090, Russia*
[3]*Novosibirsk State University, Novosibirsk, 630090, Russia*
[4]*Service d'Electromagnétisme et de Télécommunications, University of Mons, 20, pl. du Parc, B7000 Mons – Belgique Also with A. F. Ioffe Physico-Technical Institute of RAS, 26 Polytekhnicheskaya Street, St. Petersburg, 194021, Russia*
[5]*General Physics Institute RAS, Vavilov St. 38, Moscow, 119991, Russia*
**s.k.turitsyn@aston.ac.uk*

Abstract: We develop a theoretical framework for modeling of continuous wave Yb-doped fiber lasers with highly nonlinear cavity dynamics. The developed approach has shown good agreement between theoretical predictions and experimental results for particular scheme of Yb-doped laser with large spectral broadening during single round trip. The model is capable to accurately describe main features of the experimentally measured laser outputs such as power efficiency slope, power leakage through fibre Bragg gratings, spectral broadening and spectral shape of generated radiation.

OCIS codes: (190.4360) Nonlinear optics, devices; (140.3430) Laser theory.

References and links

1. A. E. Siegman, *Lasers* (University Science Books, 1986).
2. S. A. Babin, V. Karalekas, E. V. Podivilov, V. K. Mezentsev, P. Harper, J. D. Ania-Castanon, and S. K. Turitsyn, "Turbulent broadening of optical spectra in ultralong Raman fiber lasers," Phys. Rev. A **77**(3), 033803 (2008).
3. E. G. Turitsyna, G. Falkovich, V. K. Mezentsev, and S. K. Turitsyn, "Optical turbulence and spectral condensate in long-fiber lasers," Phys. Rev. A **80**(3), 031804(R) (2009).
4. D. R. Solli, C. Ropers, P. Koonath, and B. Jalali, "Optical rogue waves," Nature **450**(7172), 1054–1057 (2007).
5. J. M. Dudley, G. Genty, and B. J. Eggleton, "Harnessing and control of optical rogue waves in supercontinuum generation," Opt. Express **16**(6), 3644–3651 (2008).
6. K. Hammani, C. Finot, J. M. Dudley, and G. Millot, "Optical rogue-wave-like extreme value fluctuations in fiber Raman amplifiers," Opt. Express **16**(21), 16467–16474 (2008).
7. K. Hammani, B. Kibler, C. Finot, and A. Picozzi, "Emergence of rogue waves from optical turbulence," Phys. Lett. A **374**(34), 3585–3589 (2010).
8. A. S. Kurkov and E. M. Dianov, "Moderate-power CW fiber lasers," Quantum Electron. **34**(10), 881–900 (2004).
9. O. N. Egorova, A. S. Kurkov, O. I. Medvedkov, V. M. Paramonov, and E. M. Dianov, "Effect of the spectral broadening of the first Stokes component on the efficiency of a two-stage Raman converter," Quantum Electron. **35**(4), 335–338 (2005).
10. V. M. Paramonov, A. S. Kurkov, O. I. Medvedkov, D. A. Grukh, and E. M. Dianov, "Two-frequency fibre Raman laser," Quantum Electron. **34**(3), 213–215 (2004).
11. H. M. Pask, R. J. Carman, D. C. Hanna, A. C. Tropper, C. J. Mackechnie, P. R. Barber, and J. M. Dawes, "Ytterbium-doped silica fiber lasers—versatile sources for the 1-1.2 μm region," IEEE J. Sel. Top. Quantum Electron. **1**(1), 2–13 (1995).
12. M. Rini, I. Cristiani, and V. Degiorgio, "Numerical modeling and optimization of cascaded Raman fiber lasers," IEEE J. Quantum Electron. **36**(10), 1117–1122 (2000).
13. N. Kurukitkoson, H. Sugahara, S. K. Turitsyn, O. N. Egorova, A. S. Kurkov, V. M. Paramonov, and E. M. Dianov, "Optimisation of two-stage Raman converter based on phosphosilicate core fibre: modelling and experiment," Electron. Lett. **37**(21), 1281–1283 (2001).
14. E. M. Dianov, A. S. Kurkov, O. I. Medvedkov, V. M. Paramonov, O. N. Egorova, N. Kurukitkoson, and S. K. Turitsyn, "Raman fiber source for the 1.6-1.75 micrometer spectral region," Laser Phys. **13**(3), 397–400 (2003).
15. N. Kurukitkoson, S. K. Turitsyn, A. S. Kurkov, and E. M. Dianov, "Multiple output wavelength composite Raman fiber converter," Laser Phys. **14**(9), 1227–1230 (2004).
16. N. Vermeulen, C. Debaes, A. A. Fotiadi, K. Panajotov, and H. Thienpont, "Stokes-anti-Stokes iterative resonator method for modeling Raman lasers," IEEE J. Quantum Electron. **42**(11), 1144–1156 (2006).

#143185 - $15.00 USD Received 24 Feb 2011; revised 10 Apr 2011; accepted 11 Apr 2011; published 15 Apr 2011

17. J. C. Bouteiller, "Spectral modeling of Raman fiber lasers," IEEE Photon. Technol. Lett. **15**(12), 1698–1700 (2003).
18. J. D. Ania-Castañón, T. J. Ellingham, R. Ibbotson, X. Chen, L. Zhang, and S. K. Turitsyn, "Ultralong Raman fiber lasers as virtually lossless optical media," Phys. Rev. Lett. **96**(2), 023902 (2006).
19. J. D. Ania-Castañón, V. Karalekas, P. Harper, and S. K. Turitsyn, "Simultaneous spatial and spectral transparency in ultralong fiber lasers," Phys. Rev. Lett. **101**(12), 123903 (2008).
20. E. G. Turitsyna, S. K. Turitsyn, and V. K. Mezentsev, "Numerical investigation of the impact of reflectors on spectral performance of Raman fibre laser," Opt. Express **18**(5), 4469–4477 (2010).
21. D. V. Churkin, S. V. Smirnov, and E. V. Podivilov, "Statistical properties of partially coherent cw fiber lasers," Opt. Lett. **35**(19), 3288–3290 (2010).
22. R. Paschotta, *Encyclopedia of Laser Physics and Technology,* http://www.rp-photonics.com.
23. N. Dalloz, S. Randoux, and P. Suret, "Influence of dispersion of fiber Bragg grating mirrors on formation of optical power spectrum in Raman fiber lasers," Opt. Lett. **35**(15), 2505–2507 (2010).
24. J. M. Dudley, G. Genty, and S. Coen, "Supercontinuum generation in photonic crystal fiber," Rev. Mod. Phys. **78**(4), 1135–1184 (2006).
25. S. V. Smirnov, J. D. Ania-Castañón, T. J. Ellingham, S. M. Kobtsev, S. Kukarin, and S. K. Turitsyn, "Optical spectral broadening and supercontinuum generation in telecom applications," Opt. Fiber Technol. **12**(2), 122–147 (2006).
26. H. A. Haus, "Mode-locking of lasers," IEEE J. Sel. Top. Quantum Electron. **6**(6), 1173–1185 (2000).
27. H. A. Haus, "Theory of mode locking with a slow saturable absorber," IEEE J. Quantum Electron. **11**(9), 736–746 (1975).
28. H. A. Haus, J. G. Fujimoto, and E. P. Ippen, "Analytic theory of additive pulse and Kerr lens mode locking," IEEE J. Quantum Electron. **28**(10), 2086–2096 (1992).
29. Sh. Namiki, E. P. Ippen, H. A. Haus, and C. X. Yu, "Energy rate equations for mode-locked lasers," J. Opt. Soc. Am. B **14**(8), 2099–2111 (1997).
30. K. P. Komarov, "Theory of stationary ultrashort pulses in solid-state lasers with passive mode-locking," Opt. Spectrosc. **60**, 231–234 (1986).
31. J. N. Kutz, "Mode-locked soliton lasers," SIAM Rev. **48**(4), 629–678 (2006).
32. A. Komarov, H. Leblond, and F. Sanchez, "Multistability and hysteresis phenomena in passively mode-locked fiber lasers," Phys. Rev. A **71**(5), 053809 (2005).
33. F. O. Ilday, J. R. Buckley, W. G. Clark, and F. W. Wise, "Self-similar evolution of parabolic pulses in a laser," Phys. Rev. Lett. **92**(21), 213902 (2004).
34. F. Vanholsbeeck, St. Coen, Ph. Emplit, C. Martinelli, F. Leplingard, and T. Sylvestre, "Numerical modeling of a four-wave-mixing-assisted Raman fiber laser," Opt. Lett. **29**(23), 2719–2721 (2004).
35. T. Schreiber, B. Ortaç, J. Limpert, and A. Tünnermann, "On the study of pulse evolution in ultra-short pulse mode-locked fiber lasers by numerical simulations," Opt. Express **15**(13), 8252–8262 (2007).
36. O. Shtyrina, M. Fedoruk, S. Turitsyn, R. Herda, and O. Okhotnikov, "Evolution and stability of pulse regimes in SESAM-mode-locked femtosecond fiber lasers," J. Opt. Soc. Am. B **26**(2), 346–352 (2009).
37. B. G. Bale, S. Boscolo, J. N. Kutz, and S. K. Turitsyn, "Intracavity dynamics in high-power mode-locked fiber lasers," Phys. Rev. A **81**(3), 033828 (2010).
38. X. Tian, M. Tang, X. Cheng, P. P. Shum, Y. Gong, and C. Lin, "High-energy wave-breaking-free pulse from all-fiber mode-locked laser system," Opt. Express **17**(9), 7222–7227 (2009).
39. N. Akhmediev, J. M. Soto-Crespo, and G. Town, "Pulsating solitons, chaotic solitons, period doubling, and pulse coexistence in mode-locked lasers: complex Ginzburg-Landau equation approach," Phys. Rev. E Stat. Nonlin. Soft Matter Phys. **63**(5), 056602 (2001).
40. L. M. Zhao and D. Y. Tang, "Generation of 15-nJ bunched noise-like pulses with 93-nm bandwidth in an erbium-doped fiber ring laser," Appl. Phys. B **83**(4), 553–557 (2006).
41. A. I. Latkin, A. S. Kurkov, and S. K. Turitsyn, "Spectral broadening and power leakage in CW Yb-doped fibre laser," in *CLEO/Europe and EQEC 2009 Conference Digest* (Optical Society of America, 2009), paper CJ_P31.
42. P. Suret and S. Randoux, "Influence of spectral broadening on steady characteristics of Raman fiber lasers: from experiments to questions about the validity of usual models," Opt. Commun. **237**(1-3), 201–212 (2004).
43. V. Karalekas, J. D. Ania-Castañón, P. Harper, S. A. Babin, E. V. Podivilov, and S. K. Turitsyn, "Impact of nonlinear spectral broadening in ultra-long Raman fibre lasers," Opt. Express **15**(25), 16690–16695 (2007).
44. B. Barviau, S. Randoux, and P. Suret, "Spectral broadening of a multimode continuous-wave optical field propagating in the normal dispersion regime of a fiber," Opt. Lett. **31**(11), 1696–1698 (2006).
45. S. K. Turitsyn, E. G. Shapiro, S. B. Medvedev, M. P. Fedoruk, and V. K. Mezentsev, "Physics and mathematics of dispersion-managed optical solitons," C. R. Phys. **4**(1), 145–161 (2003).
46. A. A. Fotiadi and R. V. Kiyan, "Cooperative stimulated Brillouin and Rayleigh backscattering process in optical fiber," Opt. Lett. **23**(23), 1805–1807 (1998).
47. A. A. Fotiadi, P. Mégret, and M. Blondel, "Dynamics of a self-Q-switched fiber laser with a Rayleigh-stimulated Brillouin scattering ring mirror," Opt. Lett. **29**(10), 1078–1080 (2004).
48. A. A. Fotiadi and P. Mégret, "Self-Q-switched Er-Brillouin fiber source with extra-cavity generation of a Raman supercontinuum in a dispersion-shifted fiber," Opt. Lett. **31**(11), 1621–1623 (2006).
49. A. A. Fotiadi, R. Kiyan, O. Deparis, P. Mégret, and M. Blondel, "Statistical properties of stimulated Brillouin scattering in single-mode optical fibers above threshold," Opt. Lett. **27**(2), 83–85 (2002).
50. S. A. Babin, D. V. Churkin, A. E. Ismagulov, S. I. Kablukov, and E. V. Podivilov, "Four-wave-mixing-induced turbulent spectral broadening in a Raman fiber laser," J. Opt. Soc. Am. B **24**(8), 1729–1738 (2007).

#143185 - $15.00 USD Received 24 Feb 2011; revised 10 Apr 2011; accepted 11 Apr 2011; published 15 Apr 2011

1. Introduction

Modeling of continuous wave (CW) lasers is traditionally considered to be somewhat less complicated compared to analysis of pulsed lasers (see e.g [1]. and references therein). Stationary operation of CW lasers typically does not require consideration of temporal evolution of radiation leading to substantial simplification of modeling. However, many modern high-power, the so-called CW lasers, generate radiation output that only *on average* can be treated as a constant power wave, and as a matter of fact, is rather a pulsating irregular field. When deviations of such pulsations from an average level are not small and they do not have impact on the device performance, temporal dynamics of the radiation can be neglected and power average models can be used for description of performance of such laser systems. However, statistical oscillations of power might be directly relevant to spectral performance of laser [2,3] and might be accompanied by generation of high amplitude waves - the so-called optical rogue waves [4–7] that can potentially produce critical damage to laser systems. Though our approach and analysis will be generic in many aspects, to be specific, we will consider in what follows fibre laser systems. Averaged models dealing with an average optical power and neglecting the phase of optical field and time dynamics of the radiation are commonly used for analysis of CW fiber lasers (it is not easy to overview all literature in this field, see e.g [8–23]. and references therein). There are, however, situations when temporal behavior of "CW" laser cannot be disregarded. In high-power lasers the radiation propagating along the cavity might experience nonlinear effects. In particular, temporally modulated radiation propagating along the fibre cavity at high powers can be spectrally broadened due to nonlinear Kerr effect. Spectral broadening of the fiber laser emission can degrade system efficiency, complicate frequency doubling and is a non-desirable effect in some applications [9]. On the other hand, effect of the spectral broadening has many practical applications, e.g. it lies in a very background of the operation of supercontinuum laser sources [24,25]. It can also be used to generate multi wavelength laser outputs [10]. Study of the nonlinear spectral broadening is both an interesting fundamental and practical engineering problem relevant to laser performance. An accurate modeling of spectral broadening in the context of high-power CW lasers is a challenging numerical problem and in this work we propose and examine a simplified numerical approach to this problem.

The key model, commonly used for analysis of pulsed mode-locked femtosecond or picosecond fiber lasers (see for instance [26–40] and numerous references therein) is the modified Ginzburg-Landau equation that can be also treated as the nonlinear Shrödinger equation (NLSE) with dissipative terms. As it was mentioned above, a temporal evolution of the optical radiation might play an important role in performance of high power fiber laser also for CW lasers. We would like to point out that we do not consider any heating effects that might be important for high power laser performance and focus here only on the optical field dynamics. The key challenge in modeling of nonlinear field evolution in Fabry-Perot resonator-based CW lasers is to account correctly interaction of forward and backward propagating waves. This makes modeling of field evolution a nontrivial problem and requires numerical approaches different from methods used for ring lasers with suppressed counter propagating waves, or pulsed laser systems where interaction of forward and backward pulses can be neglected. Another important issue in the modeling of the amplitude evolution in high-power CW lasers is that a spectral broadening of powerful laser radiation might lead to large changes [41–44] of the field parameters during one round trip, breaking assumption that is typically used in the classical mode-locked laser models – that changes are small over single round trip (see e.g [26–32].). Note also that one more an important difference between modeling of mode-locking pulsed lasers and CW systems is that randomly pulsating asymptotic state of CW laser is much more complex object than a stable solitary wave pulse generated in mode-locking systems. For instance, in modeling short pulses, the numerical window might be chosen to be much smaller than the round trip because most important dynamics happen near the pulse. Considering random CW oscillations the numerical window, in general, should be broader to obtain representative statistics of the temporal field variations.

#143185 - $15.00 USD Received 24 Feb 2011; revised 10 Apr 2011; accepted 11 Apr 2011; published 15 Apr 2011

The NLSE-like models are widely used to describe spectral broadening of continuous-wave radiation, for instance, in the context of supercontinuum generation [24,25]. However, such models are less used in the context of the laser cavity configurations, because direct modeling of coupled forward and backward propagating fields in resonator presents a hybrid boundary-evolution problem that is more difficult for numerical analysis.

In this work we study experimentally and theoretically spectral broadening of radiation in CW Yb-doped fiber laser operating at 1084nm. One of the key goals of this work is to develop simplified approach based on the NLSE-like model to characterize intra-cavity evolution of laser radiation. The proposed approach allows us to account for nonlinear intra-cavity dynamics that occurs due to nonlinear Kerr effect and gain saturation. The way in which we model field evolution in fiber laser is somewhat similar to the approach widely used for modeling of periodic fiber optic communications lines [45] when NLS-like equation is being solved on each consecutive periodic section (on each round-trip in our case).

The structure of the paper is as follows. First, in section 2 we discuss the laser set-up and experimental results and describe the main features of the measured output radiation characteristics such as power, leakage through fiber Bragg grating (FBG), spectral broadening and shape of the generated spectra. In section 3 we introduce theoretical model and numerical procedure. In section 4 we discuss the results of numerical modeling and comparison with the experiment.

2. Setup and reference experimental results

Experimental setup is shown in Fig. 1 (left). The *35* meter Yb-doped fiber (GTWave) with *7μm* core was pumped with *910 nm* laser diode at up to *23W* output power.

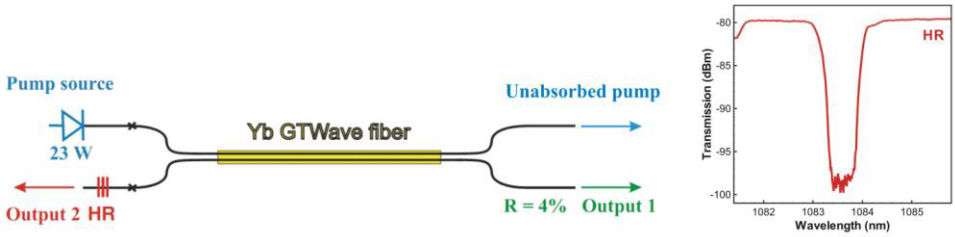

Fig. 1. (left) Experimental setup, (right) transmission spectrum.

Laser operates in CW regime with maximal output power of *12W*. The high reflectivity (HR) FBG at the left end of the cavity has maximum reflectivity at *1084nm* and spectral width of ~0.5 nm. Transmission spectrum is depicted in Fig. 1 (right). At the other end, the Fabry-Perot resonator was formed by the 4% back reflection from the fiber edge. A fraction of power leaves the cavity through leakage around FBG that can be treated as an effective "decrease of the FBGs reflectivities" [43,44,20]. The output power measurements for varying diode pump power are summarized in Fig. 2 (top). Here the green line shows the unabsorbed pumping power and blue line – the generated radiation at the 4% reflection flat end. It is seen that although the major fraction of power leaves the cavity through the flat end Fig. 2 (top right) (red rectangles), a small fraction of the generated power leaks through FBG reflector Fig. 2 (top left) (blue rectangles). The later fraction grows with the increase of pump power. Such dependence is physically transparent, since the higher pump power generates higher intra-cavity laser radiation power. This in turn leads to more nonlinear dynamics in the cavity due to Kerr nonlinearity, in particular, to larger spectral broadening. The resulting leakage of power is evidently higher for broader spectrum that bypasses the FBG reflector and leaves the resonator acting as an additional cavity loss.

#143185 - $15.00 USD Received 24 Feb 2011; revised 10 Apr 2011; accepted 11 Apr 2011; published 15 Apr 2011

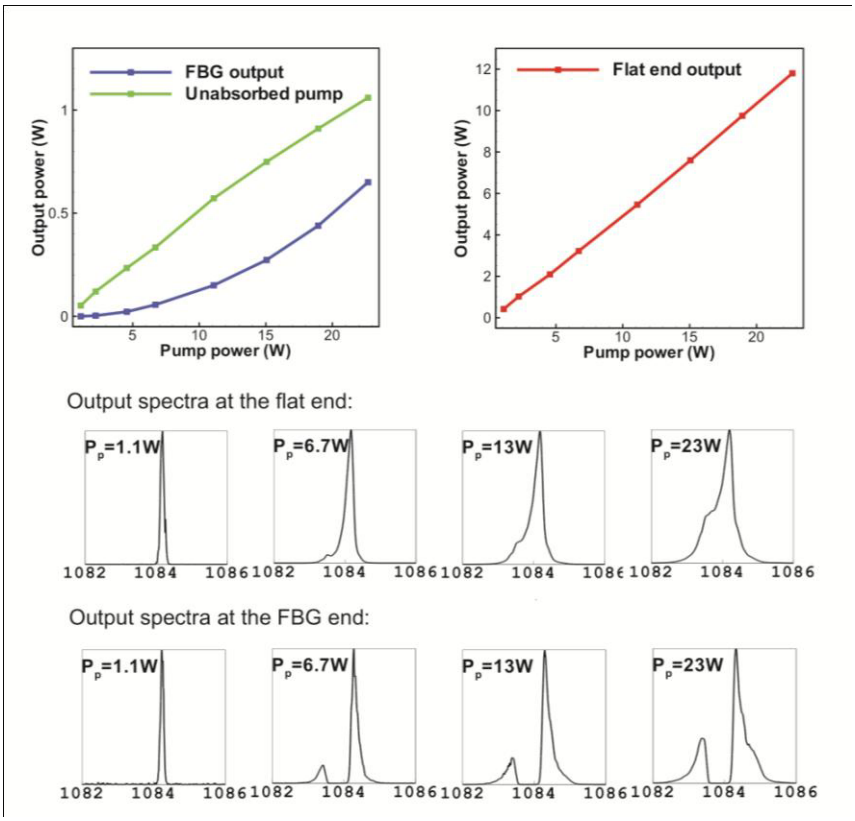

Fig. 2. (top) Measured laser output power and (middle and bottom rows) output spectra for various pumping power at the flat end and at the FBG cavity edge.

We also measured spectra of the output radiation from both FBG and the flat fiber ends of the cavity. Examples of experimentally measured spectra are shown in Fig. 2 (middle and bottom rows). At the FBG output a typical output spectrum (bottom row) has a double peaked structure due to spectral broadening and the radiation overflowing of the FBG reflector. The skew of the spectrum is due to the Brillouin scattering effect or due to an asymmetric gain spectrum of the active fiber. This asymmetry will be discussed in more detail below.

Another feature of the laser performance that can be derived from Fig. 2 (top left) (green rectangles correspond to unabsorbed pump) is that more than 95% of the pump power is absorbed inside the cavity, i.e. is transformed into laser radiation. This means that modeling should account not only for the gain saturation by laser radiation, but also for corresponding inhomogeneous gain distribution inside the cavity and distributed pump depletion.

Let us summarize the key experimental data that any adequate model should be able to reproduce. Apart from the background requirement to reproduce accurately the power efficiency conversion diagram shown in Fig. 2 (top right), there are several modeling challenges. First challenge is to reproduce quantitatively the amount of power leakage through FBG. Second fact that should be incorporated into the model is that almost all pumping power is absorbed and at the right end of the cavity (opposite to the pump source) less than 5% of the pump is left. Therefore, a spatial distribution of pumping wave should be taken into account.

3. Theory and algorithm for numerical modeling

In this section basing on the key experimental observations concerning generated laser radiation properties described above we build a simple mathematical model capable to describe phase evolution of the optical field. To model building of laser radiation in cavity over many round-trips we consider evolution of optical field in a resonator as an effective

#143185 - $15.00 USD Received 24 Feb 2011; revised 10 Apr 2011; accepted 11 Apr 2011; published 15 Apr 2011

propagation along a line that reproduces in an identical order all cavity elements periodically placed to reflect round trips circulation as shown schematically in Fig. 3. This approach has similarity with modelling of cascaded fiber-optic communication links [45]. The difference is that here we take iteratively fields propagating in the opposite direction from the previous. Note that though modelling procedure resembles models used to study mode-locked lasers [26–32], here no assumption of smallness of field changes over one period (round trip) is used. Just opposite, as it will be shown below, generated radiation experiences strong nonlinear modifications that manifest themselves through large spectral broadening. Thus, this model is capable to trace nonlinear intra-cavity evolution of the optical field that plays a major role in the performance of considered CW laser.

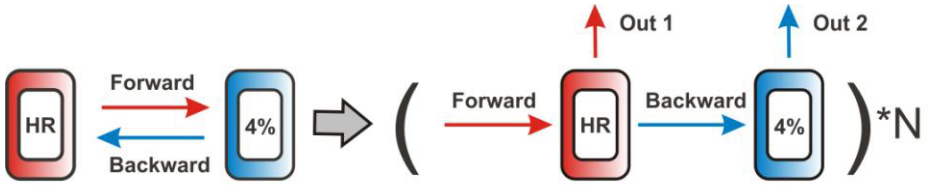

Fig. 3. Effective equivalent scheme used in modeling.

Note that applying approach that model in detail nonlinear dynamics of the generated radiation during each round trip we, certainly, are not able to get to anywhere close to millions of round trips that happen every second in a real laser, but still we can expect that after a reasonably large number of roundtrips (typically a thousand or more) main characteristics of laser radiation such as energy and spectral shape will approach some asymptotic averaged values with statistically distributed deviations. This would mean that we are operating close to the regime of stable lasing that then can be compared to the experimentally observed one. Signal evolution inside active fiber (we consider here Fabry-Perot configuration) is described by the coupled modified NLS equations with gain and loss:

$$\frac{\partial A^+}{\partial z}+\beta_1\frac{\partial A^+}{\partial t}+\frac{i\beta_2}{2}\frac{\partial^2 A^+}{\partial t^2}-i\gamma\{\left|A^+\right|^2+2\left|A^-\right|^2\}A^+=g(\left|A^+\right|^2+\left|A^-\right|^2)A^+-\frac{\alpha}{2}A^+ \quad (1)$$

$$-\frac{\partial A^-}{\partial z}+\beta_1\frac{\partial A^-}{\partial t}+\frac{i\beta_2}{2}\frac{\partial^2 A^-}{\partial t^2}-i\gamma\{\left|A^-\right|^2+2\left|A^+\right|^2\}A^-=g(\left|A^+\right|^2+\left|A^-\right|^2)A^--\frac{\alpha}{2}A^- \quad (2)$$

Here + and – corresponds, respectively, to forward and backward propagating waves.

The specific fiber parameters that are used in simulations throughout the paper are as follows: group velocity dispersion is 20 ps^2/km, nonlinearity coefficient gamma is 5$W^{-1}km^{-1}$; gray losses: for signal ~20 dB/km, for pumping wave ~50 dB/km, splicing losses for signal near the HR (1084 nm) ~10%; also we take into account that only 90% of pumping power is coupled into the fibre. Each roundtrip consists of propagation in forward and backward direction. Light is emitted from both sides of the cavity. Amplitudes of output fields:

$$A_L(\omega)=\sqrt{1-R_L(\omega)}A^-(\omega),\ A_R(\omega)=\sqrt{1-R_R(\omega)}A^+(\omega),$$

where $R_L(\omega)=R(\omega)$ and $R_R(\omega)=R_{4\%}=0.04$ are the reflectivities (with respect to power) at the left and right cavity ends correspondingly and $A(\omega)$ is an intra-cavity field. The width of the reflectivity spectrum of FBG (Fig. 1) is approximately B_λ = 0.5 nm and central wavelength is λ_0 = 1083.67nm. Total signal power $P=P^++P^-=\left|A^+\right|^2+\left|A^-\right|^2$.

Respectively, in the CW limit the power evolution of the backward and forward fields is:

#143185 - $15.00 USD Received 24 Feb 2011; revised 10 Apr 2011; accepted 11 Apr 2011; published 15 Apr 2011

$$\frac{dP^+}{dz} = g(P)P^+ - \alpha P^+ \tag{3}$$

$$-\frac{dP^-}{dz} = g(P)P^- - \alpha P^- \tag{4}$$

Gain g(P) has to be found from the material equations – typically, by solving 4-level active medium equations [8,11] (or an effective 2-level model) together with the field propagation equation. We assume that the gain is saturated with generated power and this saturation will be quantified in the next section.

3.1 An effective gain medium model: two-level system model

A model for an effective two-level system (provided that only the fibre core is doped) reads:

$$\begin{aligned}
&\frac{dN_2(z,t)}{dt} = \left(\sigma_{12}^{(p)} \rho_p(0) \frac{P_p(z)}{h\nu_p} + \sigma_{12}^{(s)} \rho_s(0) \frac{P_s^+(z) + P_s^-(z)}{h\nu_s} \right) N - \\
&- \left((\sigma_{21}^{(p)} + \sigma_{12}^{(p)}) \rho_p(0) \frac{P_p(z)}{h\nu_p} + (\sigma_{21}^{(s)} + \sigma_{12}^{(s)}) \rho_s(0) \frac{P_s^+(z) + P_s^-(z)}{h\nu_s} + \frac{1}{T_{Yb}} \right) N_2(z,t) \\
&\frac{dP_p(z)}{dz} = (\sigma_{21}^{(p)} + \sigma_{12}^{(p)}) \rho_p(0) N_2(z,t) \cdot P_p(z) - \sigma_{12}^{(p)} \rho_p(0) N \cdot P_p(z) \\
&\frac{dP_s^{\pm}(z)}{dz} = \pm (\sigma_{21}^{(s)} + \sigma_{12}^{(s)}) \rho_s(0) N_2(z,t) \cdot P_s^{\pm}(z) \mp \sigma_{12}^{(s)} \rho_s(0) N \cdot P_s^{\pm}(z)
\end{aligned} \tag{5}$$

Here index p stands for pump wave and s for the generated wave (signal); $\sigma_{12}^{(p)}$ and $\sigma_{21}^{(p)}$ are the effective pump absorption and emission cross sections, $\sigma_{12}^{(s)}$ and $\sigma_{21}^{(s)}$ are the corresponding values for the signal wavelength, $N = \int_S n(\vec{r}) d\vec{r}$ and $N_2 = \int_S n_2(\vec{r}) d\vec{r}$ - are, respectively, the total numbers of all (N) and excited Yb-ions (N_2) integrated over the fiber mode cross-section, ($n(\vec{r}), n_2(z,\vec{r})$ are corresponding Yb-ion concentrations accounted as $n(\vec{r}) = N\delta(\vec{r})$ and $n_2(\vec{r}) = N_2\delta(\vec{r})$, respectively); $\rho_P(\vec{r})$ and $\rho_S(\vec{r})$ are normalized pump and signal power distributions through fiber cross-section, so that $\int_S \rho_{P,S}(\vec{r}) d\vec{r} = 1$. The specific fiber parameters that are used in simulations throughout the paper are: $T_{Yb} = 850\,\mu s$ is the Yb-ion life time, $\sigma_{12}^{(p)} = 635 \times 10^{-27} m^2$, $\sigma_{12}^{(s)} = 1.5 \times 10^{-27} m^2$, $\sigma_{21}^{(p)} \approx 20 \times 10^{-27} m^2$, $\sigma_{21}^{(s)} = 220 \times 10^{-27} m^2$ are the effective absorption and emission cross sections; $N = 2.3 \times 10^{15} m^{-1}$ is the total numbers of Yb-ions integrated over the fiber core area, $\rho_S(0) = 1.8 \times 10^{10} m^{-2}$, $\rho_P(0) = 8.0 \times 10^7 m^{-2}$ are values of normalized pump and signal power distributions in the core center, $\alpha_s \approx 0.062 m^{-1}, \alpha_p \approx 0.115 m^{-1}$ are unsaturated absorption coefficients.

The round trip time corresponding to the experimental setup in Fig. 1 is around 340 ns and is much smaller than $T_{Yb} = 850\,\mu s$. We assume that during one round trip optical field cannot change N_2 significantly (see also discussion at the end of this section). We consider impact of the interaction of the optical fields with active medium at time scales much larger than T_{Yb}, therefore, in what follows we assume only stationary/quasi-stationary operation condition $dN_2 / dt = 0$ that leads to:

#143185 - $15.00 USD Received 24 Feb 2011; revised 10 Apr 2011; accepted 11 Apr 2011; published 15 Apr 2011

$$N_2(z)=\frac{N\left(\frac{\sigma_{12}^{(p)}\rho_p(0)}{h\nu_p}P_p(z)+\frac{\sigma_{12}^{(s)}\rho_s(0)}{h\nu_s}(P_s^+(z)+P_s^-(z))\right)}{\frac{(\sigma_{21}^{(p)}+\sigma_{12}^{(p)})\rho_p(0)}{h\nu_p}P_p(z)+\frac{(\sigma_{21}^{(p)}+\sigma_{12}^{(p)})\rho_s(0)}{h\nu_s}(P_s^+(z)+P_s^-(z))+\frac{1}{T}}$$

In this case, evolution of pump and signal powers can be described by the following set of equations:

$$\frac{dP_p(z)}{dz}=\frac{\alpha_p\frac{P_p(z)}{P_{sat}^{(p)}}+\frac{\alpha_p}{\mu}\frac{P_s^+(z)+P_s^-(z)}{P_{sat}^{(s)}}}{1+\frac{P_s^+(z)+P_s^-(z)}{P_{sat}^{(s)}}+\frac{P_p(z)}{P_{sat}^{(p)}}}P_p(z)-\alpha_p P_p(z) \tag{6}$$

$$\frac{dP_s^{\pm}(z)}{dz}=\pm\frac{\alpha_s\mu\frac{P_p(z)}{P_{sat}^{(p)}}+\alpha_s\frac{P_s^+(z)+P_s^-(z)}{P_{sat}^{(s)}}}{1+\frac{P_s^+(z)+P_s^-(z)}{P_{sat}^{(s)}}+\frac{P_p(z)}{P_{sat}^{(p)}}}P_s^{\pm}(z)\mp\alpha_s P_s^{\pm}(z)=\pm g(P)P_s^{\pm}(z)\mp\alpha_s P_s^{\pm}(z) \tag{7}$$

Here we introduced the following notations: $\alpha_s=\sigma_{12}^{(s)}\rho_s(0)N$, $\alpha_p=\sigma_{12}^{(p)}\rho_p(0)N$, $P_{sat}^{(s)}=\frac{h\nu_s}{T(\sigma_{21}^{(s)}+\sigma_{12}^{(s)})\rho_s(0)}$, $P_{sat}^{(p)}=\frac{h\nu_p}{T(\sigma_{12}^{(p)}+\sigma_{21}^{(p)})\rho_p(0)}$, $\mu^{-1}=\frac{\sigma_{12}^{(s)}}{\sigma_{12}^{(p)}}\frac{\sigma_{21}^{(p)}+\sigma_{12}^{(p)}}{\sigma_{12}^{(s)}+\sigma_{21}^{(s)}}$. One can estimate saturation powers as $P_P^{SAT}=4.9\ W$, $P_S^{SAT}\approx 55\ mW$. Note that: $\frac{\alpha_s}{\alpha_p}\frac{P_{sat}^{(s)}}{P_{sat}^{(p)}}=\mu^{-1}\frac{\nu_s}{\nu_p}$.

This set of equations should be supplemented with the following boundary conditions: $P_p(0)=P_{p0}$, $P_s^-(L)=R_R\cdot P_s^+(L)$, $P_s^-(0)=P_s^+(0)$. It is convenient to express boundary conditions through the experimentally measured output powers: $P_s(L)=P_{out}^{(s)}/(1-R_R)$, $P_p(L)=P_{out}^{(p)}/(1-R_R)$. Note, that the evolution Eqs. (6)–(7) have several conserved quantities that can help to control accuracy of numerical modelling:

1) $P_s^+(z)\cdot P_s^-(z)=P_s^+(0)\cdot P_s^-(0)$

2) After simple manipulations we can find the following relation:

$$\left[\frac{P_p(z)}{P_p(0)}\right]^{\eta}\sqrt{\frac{P_s^-(z)}{P_s^-(0)}}\Bigg/\sqrt{\frac{P_s^+(z)}{P_s^+(0)}}=\left[\frac{P_p(z)}{P_p(0)}\right]^{\eta}\left(\frac{P_s^+(z)}{P_s^+(0)}\right)^{-1}=\exp[\alpha_s(1-\mu)z]. \tag{8}$$

Here $\eta=\mu\frac{\alpha_s}{\alpha_p}=\frac{P_{sat}^{(p)}}{P_{sat}^{(s)}}\frac{\nu_s}{\nu_p}$. The signal power spatial distribution can be linked to the pump power variation through the relation:

$$P_s(z)=P_s^+(z)+P_s^-(z)=P_s^+(0)\times e^{-\alpha_s(1-\mu)z}\times\left[\frac{P_p(z)}{P_p(0)}\right]^{\eta}+P_s^-(0)\times e^{\alpha_s(1-\mu)z}\times\left[\frac{P_p(z)}{P_p(0)}\right]^{-\eta}.$$

Combining Eq. (8) with the boundary conditions (here $R=R_R$) yields:

#143185 - $15.00 USD Received 24 Feb 2011; revised 10 Apr 2011; accepted 11 Apr 2011; published 15 Apr 2011

$$\alpha_p = \frac{\alpha_s \mu \left(\ln \frac{1}{\beta} - \ln(\frac{1}{1-R}) \right)}{\alpha_s L(\mu - 1) - \ln(\frac{1}{\sqrt{R}})} \tag{9}$$

Equations (6), (7) can be re-written in a more compact way by introduction of the following notations: $P_p(z) = P_{sat}^{(p)} f(x), P_s^{\pm}(z) = P_{sat}^{(s)} h^{\pm}(x), h(x) = h^{+}(x) + h^{-}(x), x = z\alpha_s$.

$$\eta \frac{d \ln f}{dx} = \frac{-\mu + (1-\mu) h(x)}{1 + f(x) + h(x)} \tag{10}$$

$$\frac{d \ln h^{\pm}}{dx} = \pm \frac{-1 + (\mu - 1) f(x)}{1 + f(x) + h(x)} \tag{11}$$

The corresponding boundary conditions to Eqs. (10), (11) are:

$$f(0) = f_0 = P_p(0) / P_{sat}^{(p)}, h^{-}(l_0 = L\alpha_s) = R h(l_0), h^{-}(0) = h^{+}(0).$$

Resolving Eqs. (10), (11) for different μ, η it is possible to compare $P_{sat}^{(s)}$, $P_{sat}^{(p)}$, α_s and α_p with the experimental data which gives a possibility of independent cross check of the parameters of the effective 2 level model. Selection of specific η gives a relation between saturation powers of signal and pump. Parameter μ should be estimated from the known data for Yb. Power is averaged over numerical time window *T* that is in our simulation is much smaller when the roundtrip time. Indeed with the roundtrip time corresponding to the experimental setup in Fig. 1 equal to 340ns ($T_R = 2nL/c$, where $L = 35m$ is fibre length, $n = 1.45$ – refractive index, c – speed of light) such a large time window would imply very time consuming computations. We expect that averaging over the selected numerical window correctly reflects average properties of the power and we verify our approach by direct comparison with the experimental results. The use of steady-state two-level approach is a reasonable approximation for explanation of our experimental results. Indeed, the broadening the laser spectrum observed in our experiment is recorded with the spectral resolution not higher than tens of picometers. This means that power fluctuations constituting CW generation and contributing our observations possess rather short correlation times ($\tau_s << T$), typically much smaller than $\tau_s \sim 1$ ns. Such short fluctuations (positive or negative) with an amplitude δP_s contain obviously not enough energy ($\delta P_s \tau_s << P_{sat}^{(s)} T \sim 50 \mu J$) to affect in any extent the steady-state population inversion level (see (5)) established due averaging out over many such fluctuations. However, it is important to note, that the proposed model might not be sufficient to describe the laser operation in some specific regimes (such as Q-switch, Q-switch – mode-lock, or optical rouge wave generation), when a single laser pulse accumulates a significant part of the laser energy. These regimes are beyond the scope of our consideration.

3.2 Iterative propagation model

Next we describe in more detail the iterative approach used for modeling of larger spectral broadening during one round trip and building of steady state over many round trips. The main mechanism through which forward and backward propagating waves effectively interact is the gain saturation. Nonlinear interactions are suppressed due to the group velocity mismatch.

#143185 - $15.00 USD Received 24 Feb 2011; revised 10 Apr 2011; accepted 11 Apr 2011; published 15 Apr 2011

$$\frac{\partial A^{+(n)}}{\partial z}+\beta_1\frac{\partial A^{+(n)}}{\partial t}+\frac{i\beta_2}{2}\frac{\partial^2 A^{+(n)}}{\partial t^2}-i\gamma\{\left|A^{+(n)}\right|^2+2\,|\,A^{-(n-1)}\,|^2\}A^{+}=\frac{g(A^{+(n)},A^{-(n-1)})}{2}A^{+(n)}-\frac{\alpha}{2}A^{+(n)} \tag{12}$$

$$-\frac{\partial A^{-(n)}}{\partial z}+\beta_1\frac{\partial A^{-(n)}}{\partial t}+\frac{i\beta_2}{2}\frac{\partial^2 A^{-(n)}}{\partial t^2}-i\gamma\{\left|A^{-(n)}\right|^2+2\,|\,A^{+(n-1)}\,|^2\}A^{-}=\frac{g(A^{+(n)},A^{-(n)})}{2}A^{-(n)}-\frac{\alpha}{2}A^{-(n)} \tag{13}$$

where n is the roundtrip number, z varies from *0* to L and these equations are coupled through

$$g(P^{+},P^{-})=\frac{\alpha_s\,\mu\,\dfrac{P_p(z)}{P_{sat}^{(p)}}+\alpha_s\dfrac{P^{+}(z)+P^{-}(z)}{P_{sat}^{(s)}}}{1+\dfrac{P^{+}(z)+P^{-}(z)}{P_{sat}^{(s)}}+\dfrac{P_p(z)}{P_{sat}^{(p)}}},\quad P^{\pm}(z)=\frac{1}{T}\int\left|A^{\pm}(z,t)\right|^2 dt \tag{14}$$

Derived model accounts not only for gain saturation by laser radiation, but also for pump depletion. Pump distribution over the fiber length $P_p(z)$ is found by solving Eq. (6) together with the amplitude Eqs. (12)–(13). Note that, strictly speaking, system (12)–(13) is not a system of equations in mathematical sense, i.e. we don't solve these equations simultaneously. We solve the equations for forward and backward propagating waves one by one it the following order: $\ldots A_b^{(n-1)}(z,t)$, $A_f^{(n)}(z,t)$, $A_b^{(n)}(z,t)$, $A_f^{(n+1)}(z,t)\ldots$, i.e. forward propagating wave on the n-th roundtrip interacts with backward propagating wave on the (n-1)-th roundtrip which is already computed. The boundary conditions read:

$$A_f^{(n)}(0,t)=\sqrt{R_{4\%}}\cdot A_b^{(n-1)}(L,t),\ A_b^{(n)}(0,\omega)=\sqrt{R(\omega)}\cdot A_f^{(n)}(L,\omega) \tag{15}$$

Thereby, the Eqs. (12)–(13) with expression for gain (14) and boundary conditions (15) present the consistent closed iterative model, which is capable to accurately describe leakage through fibre Bragg gratings, spectral broadening and spectral shape of generated radiation.

4. Results and discussions

In this section we analyze results obtained by using the introduced model and compare where possible them to the experimental data. Typical distribution of the intra-cavity power of laser radiation (over the distance of one roundtrip *2L = 70m*) is shown in Fig. 4.

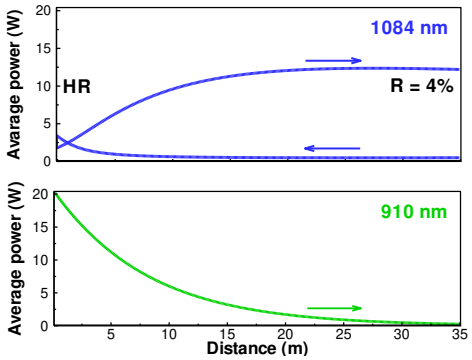

Fig. 4. Power distribution inside laser cavity for maximal pump power (22.6 W at z = 0).

Figure 5 depicts comparison of numerical modeling with the experimental results for the output power versus pump power.

#143185 - $15.00 USD Received 24 Feb 2011; revised 10 Apr 2011; accepted 11 Apr 2011; published 15 Apr 2011

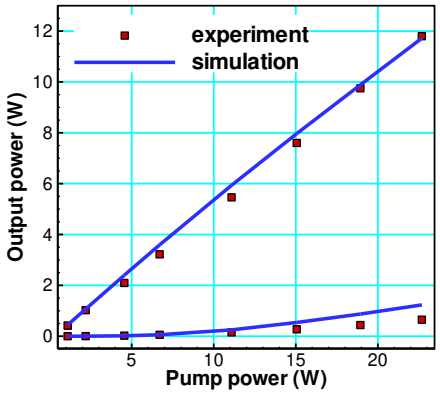

Fig. 5. Computed and measures output power as a function of pump at z = 0. Upper curve shows the output through the flat end, bottom curve correspond to the leakage through FBG.

The calculated output spectra are shown in Fig. 6. Similar to Fig. 2, the upper row here stands for the flat end and the bottom row for the FBG edge of the cavity. At right side of the cavity FBG cuts the central part of the radiation spectrum which then experiences nonlinear phase shift due to Kerr effect and leaves the cavity through the flat end. The spectra for high powers radiation leaving the resonator through the flat end (upper row) demonstrate features typical to the optical wave propagation in nonlinear fiber. We can conclude, therefore, that apart from the asymmetry spectra in simulations demonstrate the same behaviour as in the experiment, i.e. our model accurately describes nonlinear spectral broadening inside the laser cavity and power leakage through the FBG.

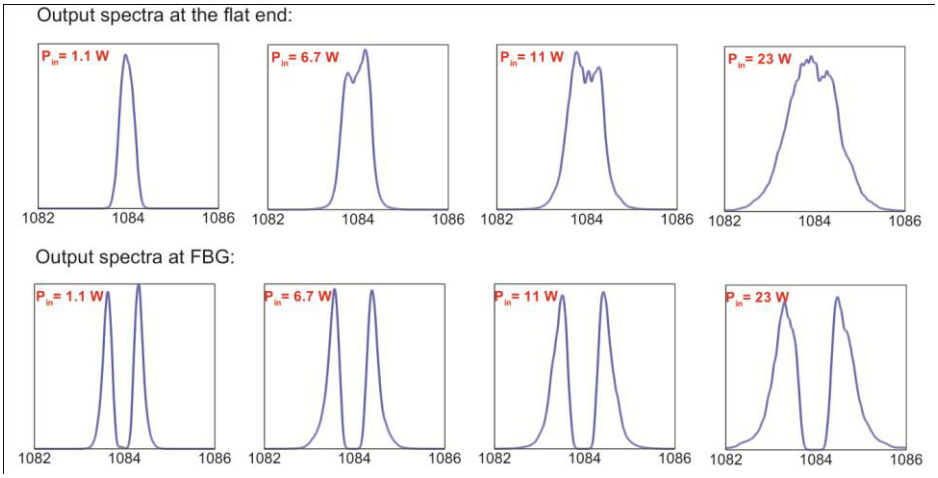

Fig. 6. Output spectra as a function of pumping power.

Pronounced asymmetry of the spectrum broadening observed in the experiment (Fig. 2) could be attributed to a specific dispersion of the FBG mirror [23]. However, the asymmetry can also result from the effect of stimulated Brillouin scattering (SBS) in the fiber laser cavity. Although a detailed quantitative description of this mechanism in the considered system (that is different from the previously developed for pulsed fiber lasers [46–49]) is beyond the scope of this paper and the SBS process is not accounted by our present model, we believe that the qualitative picture of the non-uniform line broadening can be explained by the following simplified consideration, which is supported by our experimental observations. A balance between the double-pass gain and the losses in the fiber laser cavity provides lasing of the

#143185 - $15.00 USD Received 24 Feb 2011; revised 10 Apr 2011; accepted 11 Apr 2011; published 15 Apr 2011

longitude cavity modes within the FBG reflectivity band. Four-wave-mixing between these modes through the fiber Kerr nonlinearity is responsible for symmetrical laser line broadening [50,2,3,17] as it is seen in Fig. 6. However, apart from the Kerr nonlinearity, the cavity modes could undergo a collective parametric interaction through the SBS process, i.e. a resonance coupling between the optical modes and hyper-sound standing waves induced in the fiber media. Due to the SBS resonance this coupling is pronounced for laser modes spectrally separated from each other exactly (with the accuracy of few MHz) by the SBS shift Δ_{SBS}, i.e. the frequency of the resonantly induced hyper-sound wave. Under the conditions of full resonance all such modes pairs produce the same interference pattern, i.e. all of them contribute the same pattern of electrostrictive force wave generating the phase-matched hyper-sound wave. During this resonance interaction the cavity modes that are Stokes shifted relatively the lasing modes (within the FBG reflectivity spectrum) acquire an additional Brillouin gain at the expense of the anti-Stokes shifted modes. This causes a slight redistribution of the laser gain profile in favor of modes with the longer wavelengths providing them preferable conditions for lasing. As a result, the laser modes leaked from the right side of the FBG spectra (see Fig. 2) exhibits slightly higher powers than the modes leaked from the left side.

There are two obvious observations in our experiment that support this explanation. First, the laser power accumulated inside the fiber cavity significantly exceeds the Brillouin threshold power associated with the given cavity length and fiber parameters. We can roughly estimate the SBS threshold in our cavity to be as low as 100mW, so the presence of 12W radiation inside the cavity ensures an efficient interaction of the laser modes through the SBS process. Second, an asymmetric enhancement of the modes leaked from the right side of the FBG reflectivity spectrum (Fig. 2) is observed with a shift of ~0.08 nm from the FBG reflectivity band that is in a good agreement with the SBS frequency shift $\Delta_{SBS} \approx 16GHz$ estimated for laser operating at ~1.08μm [47]. Besides, our qualitative picture agrees with a theoretical and numerical model that we recently developed and will be described elsewhere. The numerical simulations have been performed on a computational cluster of the Novosibirsk University Scientific Computing Centre. Each cluster node is a dual processor server equipped with Intel Xeon 5355 processors. Typical computational time for a single run was about an hour.

5. Conclusions

We have developed a theoretical model for the description of the performance of CW fiber lasers with large nonlinear single path dynamics manifesting itself through spectral broadening of radiation. The proposed model shows good agreement with the experimental results. We believe that the proposed approach based on combination of the nonlinear Shrödinger equations and simplified material equations for the gain medium can be used for characterization of the strongly nonlinear evolution of intra-cavity laser radiation in a range of high power lasers.

Acknowledgments

Authors would like to acknowledge the support of the UK Engineering and Physical Sciences Research Council (EPSRC), The Royal Society, The Leverhulme Trust, European FP7 IRSES project, IAPVI/10 project of the Belgian Science Policy, FEDER-Wallonia “Mediatic” project and the research grant of the Russian Federation Government N11.G34.31.0035.

#143185 - $15.00 USD Received 24 Feb 2011; revised 10 Apr 2011; accepted 11 Apr 2011; published 15 Apr 2011